

Nonlinear Regression Models to Identify Functional Forms of Deforestation in East Asia

Shojiro Tanaka, *Member, IEEE*, and Ryuei Nishii, *Member, IEEE*

Abstract—Identification of the factors involved in deforestation could lead to a comprehensive understanding of deforestation on a broad scale, as well as prediction capability. In this paper, regression models with two explanatory variables—human population and relief energy, i.e., the difference between the maximum and minimum altitudes in a sampled area—were verified as to whether they could elucidate aspects of deforestation. The functional forms of the nonlinear regression models were estimated by step functions analyzed with the use of high-precision Japanese data. Candidate smooth regression models were then derived from the obtained sigmoidal shapes by the step functions. Models with spatially dependent errors were also developed. Akaike's information criterion was used to evaluate the models on four data sets for the East Asia region. From the evaluation, we selected the best three models that systematically showed the best relative appropriateness to the real data.

Index Terms—Akaike's information criterion (AIC), forest-human interactions, human population, relief energy, sigmoidal curves, spatially dependent regression models.

I. INTRODUCTION

REMOTELY sensed measurements made by multispectral sensors and microwave radiometers are making it possible to acquire terabyte-scale information on ozone concentration [1], water vapor [2], [3], soil moisture [4], etc., as well as a complement to traditional land-cover and surface-temperature measurements. Yet, the interrelations between such information and other data have not been sufficiently studied in terms of statistical models that attempt to show socioeconomic causality with respect to changes in terrestrial surfaces [5].

Land cultivated for cash crops, cattle grazing, shifting cultivation, logging, and fuelwood use in developing countries, as well as airborne pollutants and acid rain in developed nations, are major causes of deforestation [6]. Almost all of the causes of deforestation are related to human activities [5]. Forest fires are thought to be the biggest cause of deforestation in places such as Indonesia; such fires often result from the activities of nearby human populations, e.g., unextinguished embers of bonfires, cigarettes, etc. [7].

We incorporated the human factor of population into the forest coverage ratio by using grid-cell data. We assumed that the

Manuscript received October 29, 2008; revised February 5, 2009. First published April 28, 2009; current version published July 23, 2009. This work was supported by Grant-in-Aid for Scientific Research (B) 19300093.

S. Tanaka is with the Faculty of Science and Engineering, Shimane University, Matsue 690-8504, Japan (e-mail: tanaka@cis.shimane-u.ac.jp).

R. Nishii is with the Faculty of Mathematics, Kyushu University, Fukuoka 812-8581, Japan (e-mail: nishii@math.kyushu-u.ac.jp).

Color versions of one or more of the figures in this paper are available online at <http://ieeexplore.ieee.org>.

Digital Object Identifier 10.1109/TGRS.2009.2015659

	$(x, y - 1)$	
$(x - 1, y)$	(x, y)	$(x + 1, y)$
	$(x, y + 1)$	

- $s = (x, y)$
- $F = F(s)$: forest areal ratio ($0 < F \leq 1$)
- $N = N(s) \geq 0$: human population density
- $R = R(s) \geq 0$: relief energy (meter)

cell size of Japan dataset: $\cong 1 \text{ km}^2$
cell size of world dataset: $\cong 37 \text{ km}^2$

Fig. 1. Site specification in the grid-cell system and variables on the site.

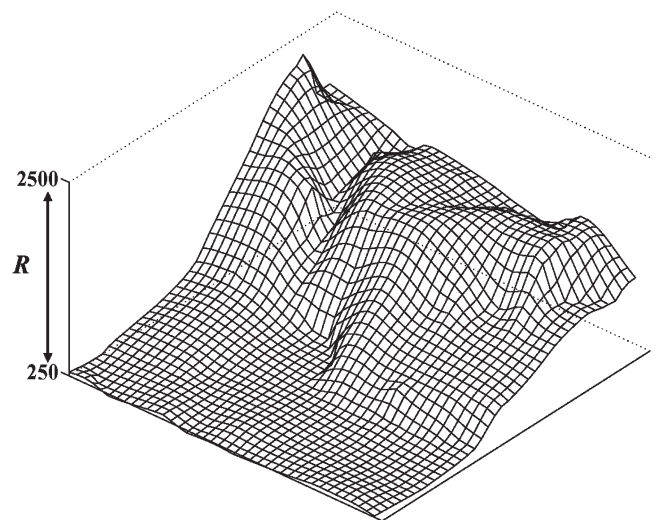


Fig. 2. Relief energy R .

process of deforestation has strong dependence on the human population in the area. Although human-related factors such as land price and availability of transportation are potentially related to deforestation, we chose human population to be the first factor to be scrutinized. Forests tend to remain on steep hillsides in populated areas since those areas are not suitable for cultivation or residence and are necessary to prevent landslides. We, hence, considered a second factor of slope steepness. Data on these two factors as well as on worldwide forest coverage are available in the form of grid cells (Fig. 1).

Let $N = N(s)$ be the population and $R = R(s)$ be the relief energy at site s . Here, the relief energy means the difference between the maximum and minimum altitudes (see Fig. 2). Also, let $F = F(s)$ be the forest areal ratio, including the open forest ($0 < F \leq 1$). $F = 0$ values are excluded because of the technical difficulty of making a distinction between bare land, desert, or water bodies in the data set described in Section V. Our main concern here is to specify a regression model of F by explanatory variables: human population N and relief energy R .

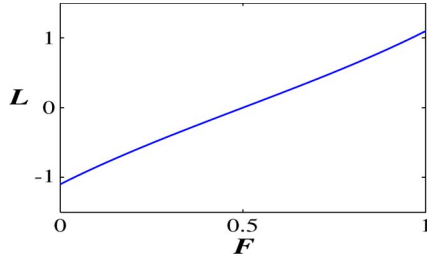


Fig. 3. eLogit transform from F to L .

We suppose an additive model of the form [8]

$$F = g(N) + h(R) + \text{error}. \quad (1)$$

In our case, forest ratio F is restricted to values from 0 to 1. Hence, the predicted values of F based on the additive model will exceed this limit in many cases. Furthermore, the logit transform $\text{Logit}(F) = \log\{F/(1-F)\}$ is not useful because it cannot deal with the data on full forest coverage with $F = 1$ [9].

Hence, a general logit transform $\log\{(F + \kappa)/(1 - F + \lambda)\}$ was proposed [10]. However, additive models of the transformed data are not appropriately evaluated since Akaike's information criterion (AIC) of the models diverges to $-\infty$ as λ tends to $+0$ due to the data with $F = 1$.

We, therefore, used the following extended logit (eLogit) transformation [11]:

$$\text{eLogit}(F) \equiv \log \frac{F + 0.5}{1 - F + 0.5} (= L). \quad (2)$$

Note that the above transformation is monotone increasing and approximately linear (Fig. 3). It transforms the interval $[0, 1]$ into $[-\log 3, \log 3]$.

In what follows, we discuss the additive model

$$\text{eLogit}(F) = g(N) + h(R) + \text{error} \quad (3)$$

where $g(\cdot)$ and $h(\cdot)$ are given by step functions or nonlinear regression functions. The inverse transformation of (3) is given by

$$F = 1.5 - \frac{2}{1 + \exp\{g(N) + h(R) + \text{error}\}}. \quad (4)$$

This paper unified our previous works [8]–[12] and added entire elucidation of our methodology and the refined estimations. In particular, step functions with spatially dependent errors were considered. The parameters were estimated in closed forms (without using iterative procedure; see Appendix I), and the step functions were numerically compared with other nonlinear regression models. Furthermore, new consideration is made in Section VII.

The remaining parts of this paper are organized as follows. In Section II, the two functional forms of $g(N)$ and $h(R)$ are thoroughly analyzed by regression functions using a high-precision

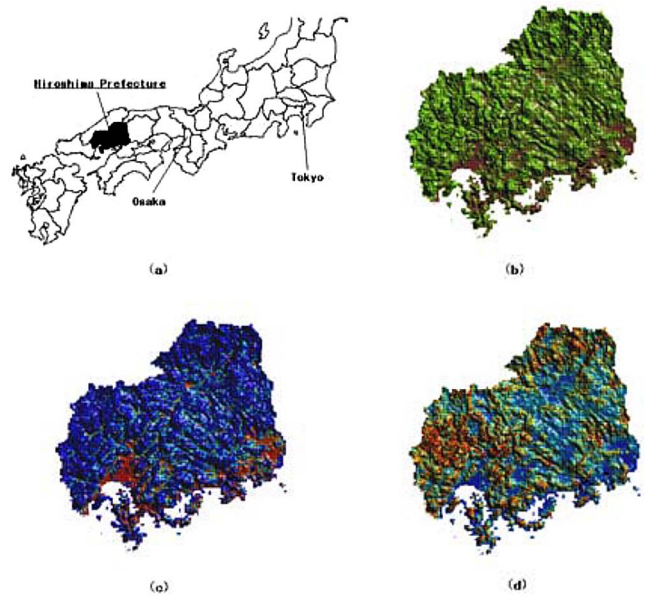


Fig. 4. Location of the test field and variable maps. (a) Test field. (b) Forest coverage ratio F . (c) Population density N . (d) Relief energy R . In maps (b) to (d), the altitude is overlaid with the corresponding variables.

TABLE I
BASIC STATISTICS OF 1-km² RESOLUTION HIROSHIMA DATA

Variable	Average value	Minimum value	Maximum value	Standard deviation
F	0.7874	1.138×10^{-4}	1.000	2.446×10^{-1}
L	0.6177	-1.098	1.099	5.292×10^{-1}
N	288.8	0.000	2.207×10^4	1.091×10^3
R	157.1	0.000	5.800×10^2	8.452×10^1

($0 < F \leq 1$, sample size: 8538)

Japanese data set with a spatial resolution of 1 km². Section III develops spatially dependent models and parameter estimation procedures. Section IV describes how the three best models were selected with the use of the high-precision Japanese data. Section V shows how the worldwide data sets were prepared and how the test areas were selected. Section VI analyzes the models best fitting the real data. Section VII concludes this paper by discussing the spatial models' superiority, the implications of the models, and the significance of the parameter estimation in developing a comprehensive understanding of forest–human interrelations.

II. REGRESSION FUNCTIONS WITH INDEPENDENT ERRORS

We first examined model (3) for the forest areal ratio with the range $0 < F \leq 1$ and human population density N in the test field of Hiroshima Prefecture in western Japan. These data have high precision, and they were created for land-use management and national census purposes. Fig. 4 illustrates the location of the test field and shows the spatial maps of the variables. Table I lists the basic statistics of the data set. The reader can consult [13] to see how the data were prepared.

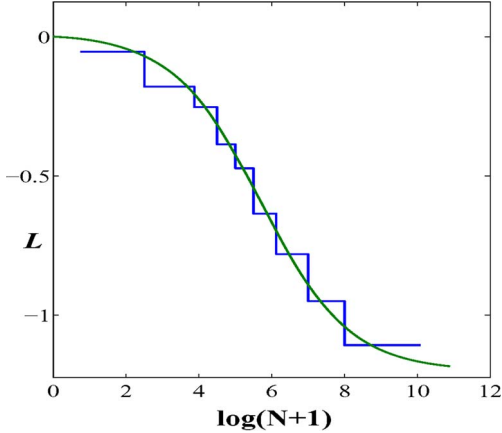


Fig. 5. Estimated step function $g_0(N)$ and smooth function $g_2(N)$ versus $\log(N+1)$.

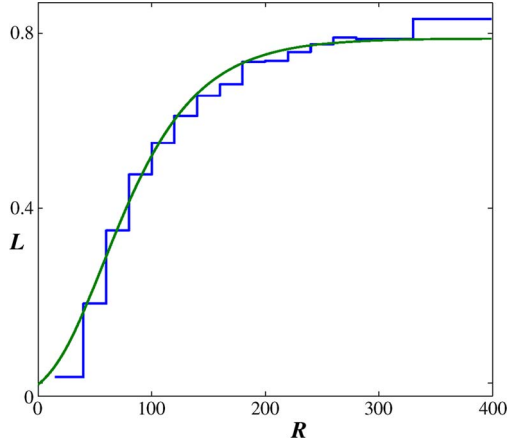


Fig. 6. Estimated step function $h_0(R)$ and smooth function $h_3(R)$ versus R .

A. Identification of Functional Forms

We need to specify the functional forms of $g(N)$ and $h(R)$. We first approximate the effect of $g(N)$ due to population N by a step function $g_0(N)$. Let $(n_0, n_1, n_2, \dots, n_9) = (0, 3, 4, 4.5, 5, 5.5, 6, 7, 8, \infty)$ be ten terminal points of intervals, and let $g_0(N)$ take a constant value ψ_i if $\log(N+1)$ belongs to interval $[n_i, n_{i+1})$ for $i = 0, 1, \dots, 8$, i.e.,

$$g_0(N) = \sum_{i=0}^8 \psi_i \cdot I(\log(N+1) \in [n_i, n_{i+1})) \quad (5)$$

where $I(\cdot)$ denotes the indicator function. These terminal points balance the sample sizes in the respective intervals. Here, ψ_0 is set to zero as a baseline.

Next, we approximate $h(R)$ by a step function $h_0(R)$. Let $(r_0, r_1, r_2, r_3, \dots, r_{15}, r_{16}) = (0, 20, 40, 60, \dots, 300, \infty)$ be the terminal points and define

$$h_0(R) = \sum_{i=0}^{15} \omega_i \cdot I(R \in [r_i, r_{i+1})). \quad (6)$$

Again, ω_0 is set to zero as a baseline.

Figs. 5 and 6 depict the estimated step functions. In Fig. 5, the estimated $g_0(N)$ has a sigmoid shape. In Fig. 6, the estimated $h_0(R)$ has a logarithmic shape. Our aim is to find the nonlinear

TABLE II
REGRESSION FUNCTIONS FOR ELOGIT MODEL

$g_0(N)$	=	step func.
$g_1(N)$	=	$-\alpha \log(N+1)$
$g_2(N)$	=	$-\frac{\beta_1}{1 + \exp\{\beta_2 - \beta_3 \log(N+1)\}} + \frac{\beta_1}{1 + \exp(\beta_2)}$
$g_3(N)$	=	$\beta [1 - \exp\{\alpha \log(N+1)\}]$
$h_0(R)$	=	step func.
$h_1(R)$	=	$I(R > \theta) \cdot \delta \log(R - \theta + 1)$
$h_2(R)$	=	$I(R > \theta) \cdot \delta \log\left(\frac{R}{\theta}\right)$
$h_3(R)$	=	$\gamma_3 \exp(-\gamma_1 e^{-\gamma_2 R}) - \gamma_3 \exp(-\gamma_1)$
$h_4(R)$	=	$\frac{\gamma_1}{1 + \exp(\gamma_2 - \gamma_3 R)} - \frac{\gamma_1}{1 + \exp(\gamma_2)}$

regression models that best fit the data. Thus, they should well approximate the estimated step functions. Therefore, we restricted our attention to the candidate models listed in Table II. Note that $g_i(N)$ are decreasing functions of N , $i = 1, 2, 3$, and $h_j(R)$ are increasing functions of R , $j = 1, \dots, 4$. It holds that $g_i(0) = h_j(0) = 0$.

The estimated smooth curves due to $g_2(N)$ and $h_3(R)$ are overlaid in Figs. 5 and 6. It is apparent that they satisfactorily approximate the step functions.

B. Model Selection With High-Precision Japanese Data

We shall evaluate all possible combinations of the candidate models in Table II, i.e.,

$$L = \log \frac{F + 0.5}{1.5 - F} = \beta_0 + g_k(N) + h_l(R) + e \quad (7)$$

where $k = 0, 1, 2, 3$, $l = 0, 1, 2, 3, 4$, and β_0 is the intercept. The initial values for parameter estimation were carefully determined from several trials.

Many criteria to select the best model in the regression have been proposed in the literature, and it is known that cross validation, final prediction error, and AIC have the same asymptotic properties (see, e.g., [14]). AIC prefers the model that minimizes the value. For a normal regression model, it is known that AIC reduces to $n \log \hat{\sigma}^2 + 2p$, where n , $\hat{\sigma}^2$, and p denote the sample size, the maximum-likelihood estimate of the variance σ^2 [15], and the total number of parameters, respectively.

III. REGRESSION FUNCTION WITH DEPENDENT ERRORS

Here, we illustrate the parameter estimation in a four-neighbor case, first for a rectangular region with a regular lattice and then for nonrectangular areas that would occur in practice.

A. Spatial Models for Complete Data Over a Rectangular Region

Consider a rectangular region of size $r \times c$, e.g., Fig. 7 with $r = 5$ and $c = 4$. Let L_{xy} be the eLogit-transformed forest coverage ratio at the image coordinate (x, y) for $x = 1, 2, \dots, r$; $y = 1, 2, \dots, c$. We define $\mathbf{L} = (L_{11}, \dots, L_{rc})^T : n \times 1$ with $n = rc$. Let $\mu_{xy} = \mu_{xy}(\boldsymbol{\beta}) = \beta_0 + g(N_{xy}; \boldsymbol{\beta}_1) +$

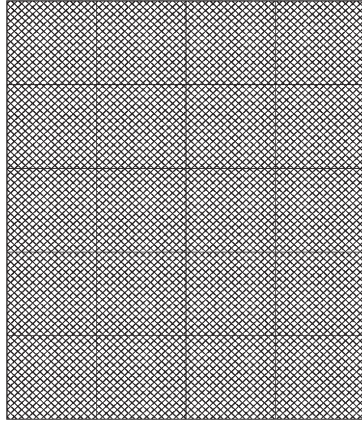


Fig. 7. Region with complete data.

$h(R_{xy}; \beta_2)$ be an expected value $E(L_{xy})$ given by a regression function with a parameter vector $\beta = (\beta_0, \beta_1^T, \beta_2^T)^T$. For example, $g(N_{xy}; \beta_1) = g_2(N)$ with $\beta_1 = (\beta_1, \beta_2, \beta_3)^T$ and $h(R; \beta_2) = h_3(R)$ with $\beta_2 = (\gamma_1, \gamma_2, \gamma_3)^T$ (see Table II for the details of parameters).

Moreover, let H be an $n \times n$ adjacency matrix whose entries correspond to the sites defined by

$$H((x, y), (x', y')) = \begin{cases} 1 & \text{if the distance between sites located} \\ & \text{at } (x, y) \text{ and } (x', y') \text{ is equal to 1} \\ 0 & \text{otherwise.} \end{cases}$$

Namely, the entries of H are 1 if two sites are adjacent, and 0 otherwise. Hence, H is symmetric, and the sum of a row is equal to four if the row corresponds to the inner points of the rectangle.

The adjacency matrix of complete data can simply be expressed by using the Kronecker product. For the example of the

complete data over Fig. 7, the adjacency matrix is given by (8) and (9), shown at the bottom of the page, where \mathbf{I} denotes the identity matrix, and

$$A_4 = \begin{pmatrix} 0 & 1 & 0 & 0 \\ 1 & 0 & 1 & 0 \\ 0 & 1 & 0 & 1 \\ 0 & 0 & 1 & 0 \end{pmatrix} \quad A_5 = \begin{pmatrix} 0 & 1 & 0 & 0 & 0 \\ 1 & 0 & 1 & 0 & 0 \\ 0 & 1 & 0 & 1 & 0 \\ 0 & 0 & 1 & 0 & 1 \\ 0 & 0 & 0 & 1 & 0 \end{pmatrix}. \quad (10)$$

We assume that the eLogit-transformed ratio L_{xy} depends on the adjacent pixels. Put $e_{xy} = L_{xy} - \mu_{xy}(\beta)$ (error). Now, let us consider the following conditional normal model:

$$\begin{aligned} L_{xy} | \{L_{x+1,y}, L_{x-1,y}, L_{x,y+1}, L_{x,y-1}\} \\ \sim \mathbf{N}(\mu_{xy} + \phi(e_{x+1,y} + e_{x-1,y} + e_{x,y+1} + e_{x,y-1}), \sigma^2). \end{aligned} \quad (11)$$

The parameter ϕ captures the spatial dependence. If $\phi = 0$, model (11) reduces to the ordinary regression model with independent errors. If $\phi > 0$ is large, the spatial dependence becomes strong.

In this case, AIC is obtained as

$$\begin{aligned} \text{AIC} = n \log(2\pi e) + n \log \hat{\sigma}^2(\hat{\phi}) - \log |\mathbf{I}_n - \hat{\phi}H| + 2p \\ - 2n \log 2 + 2 \sum_{x=1}^r \sum_{y=1}^c \log \{(F_{xy} + 0.5)(1.5 - F_{xy})\} \end{aligned} \quad (12)$$

where $\hat{\phi}$ and $\hat{\sigma}^2(\hat{\phi})$ are estimates of dependence parameter ϕ and error variance, respectively, and p denotes a total number of unknown parameters— $\mu(\beta)$, σ^2 , and ϕ —specifying nonlinear regression models (11). Here, F_{xy} are the raw forest areal rates. See Appendix I for the derivation of AIC (12).

$$H = \left(\begin{array}{ccccccccccccc} 0 & 1 & 0 & 0 & 1 & 0 & 0 & 0 \\ 1 & 0 & 1 & 0 & 0 & 1 & 0 & 0 \\ 0 & 1 & 0 & 1 & 0 & 0 & 1 & 0 \\ 0 & 0 & 1 & 0 & 0 & 0 & 0 & 1 \\ 1 & 0 & 0 & 0 & 0 & 1 & 0 & 0 & 1 & 0 & 0 & 0 \\ 0 & 1 & 0 & 0 & 1 & 0 & 1 & 0 & 0 & 1 & 0 & 0 \\ 0 & 0 & 1 & 0 & 0 & 1 & 0 & 1 & 0 & 0 & 1 & 0 \\ 0 & 0 & 0 & 1 & 0 & 0 & 1 & 0 & 0 & 0 & 1 & 0 \\ & & & 1 & 0 & 0 & 0 & 0 & 1 & 0 & 0 & 0 & 0 \\ & & & 0 & 1 & 0 & 0 & 1 & 0 & 1 & 0 & 0 & 0 \\ & & & 0 & 0 & 1 & 0 & 0 & 1 & 0 & 0 & 1 & 0 \\ & & & 0 & 0 & 0 & 1 & 0 & 0 & 1 & 0 & 0 & 1 \\ & & & & 1 & 0 & 0 & 0 & 0 & 1 & 0 & 0 & 0 & 0 \\ & & & & 0 & 1 & 0 & 0 & 1 & 0 & 1 & 0 & 0 & 0 \\ & & & & 0 & 0 & 1 & 0 & 0 & 1 & 0 & 0 & 1 & 0 \\ & & & & 0 & 0 & 0 & 1 & 0 & 0 & 1 & 0 & 0 & 1 \\ & & & & & 1 & 0 & 0 & 0 & 0 & 1 & 0 & 0 & 0 & 0 \\ & & & & & 0 & 1 & 0 & 0 & 1 & 0 & 1 & 0 & 0 & 0 \\ & & & & & 0 & 0 & 1 & 0 & 0 & 1 & 0 & 0 & 1 & 0 \\ & & & & & 0 & 0 & 0 & 1 & 0 & 0 & 1 & 0 & 0 & 1 \\ & & & & & & 1 & 0 & 0 & 0 & 0 & 1 & 0 & 0 & 0 & 0 \\ & & & & & & 0 & 1 & 0 & 0 & 1 & 0 & 1 & 0 & 0 & 0 \\ & & & & & & 0 & 0 & 1 & 0 & 0 & 1 & 0 & 0 & 1 & 0 \\ & & & & & & 0 & 0 & 0 & 1 & 0 & 0 & 1 & 0 & 0 & 1 \\ & & & & & & & 1 & 0 & 0 & 0 & 0 & 1 & 0 & 0 & 0 & 0 \\ & & & & & & & 0 & 1 & 0 & 0 & 1 & 0 & 1 & 0 & 0 & 0 \\ & & & & & & & 0 & 0 & 1 & 0 & 0 & 1 & 0 & 1 & 0 & 0 \\ & & & & & & & 0 & 0 & 0 & 1 & 0 & 0 & 1 & 0 & 0 & 1 \end{array} \right) \quad (8)$$

$$= A_5 \otimes \mathbf{I}_4 + \mathbf{I}_5 \otimes A_4 \quad (9)$$

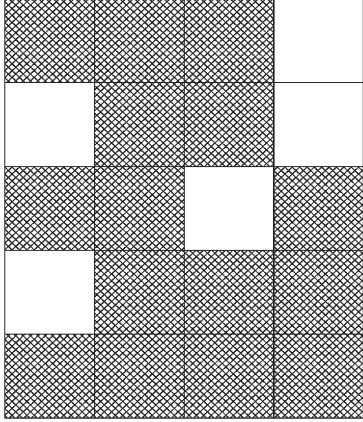


Fig. 8. Region with missing data.

TABLE III

AIC EVALUATION OF REGRESSION MODELS FOR RAW F . MODELS
 $F = \beta_0 + g(N) + h(R)$; HIROSHIMA DATA, $0 < F \leq 1$,
SAMPLE SIZE = 8538; AIC + **35904.03** TABULATED

	h_0	h_1	h_2	h_3	h_4
g_0	1884.72	1949.56	1991.94	1909.17	1937.78
g_0 spatial	1877.68	—	—	—	—
g_1	2484.19	2570.38	2701.00	2540.88	2571.60
g_2	1801.99	1938.48	1933.93	1849.74	1874.68
g_2 spatial	—	—	1357.04	1352.48	1379.68
g_3	1990.77	2097.73	2144.87	2044.28	2068.72

For a spatial model with a nontransformed raw ratio F , AIC is simply given by

$$\text{AIC} = n \log(2\pi e) + n \log \hat{\sigma}^2(\hat{\phi}) - \log |\mathbf{I}_n - \hat{\phi}H| + 2p$$

where $\hat{\sigma}^2(\hat{\phi})$ and $\hat{\phi}$ are parameters estimated by raw ratios F_{xy} 's, and they are different from those in (12).

B. Spatial Models for a Nonrectangular Region

Most municipal boundaries and interior holes like lakes do not always have a rectangular shape. One method for dealing with such irregularity is to remove the data on the edge (as if to peel off an outer shell) and to use only the sites that have four neighbors. However, this strategy loses much information. Figs. 7 and 8 illustrate how to find the adjacency matrix to make effective use of the data. This procedure is illustrated in Appendix II. The parameter estimation is carried out in a similar fashion to the one in Appendix I.

Our high-precision data set with $n = 8538$ is embedded in the rectangular grid measuring 130×115 , and the adjacency matrix was derived with the process.

IV. SELECTED MODELS USING HIGH-PRECISION DATA

Tables III and IV show the regression models for the raw ratio $0 < F \leq 1$ and for the eLogit-transformed data L , respectively. Twenty candidate models $g_k(N) + h_l(R)$ with independent errors are estimated. Furthermore, the four models with a dependent error (denoted by *spatial* in the first columns) are fitted. The AIC values in the two tables are differences from 35 904.03, the AIC obtained by the spatial model $g_2 + h_2$ for the transformed ratio. A positive AIC value means that the

TABLE IV
AIC EVALUATION OF MODELS FOR eLOGIT TRANSFORMED F . MODELS
 $L = \beta_0 + g(N) + h(R)$; HIROSHIMA DATA, $0 < F \leq 1$,
SAMPLE SIZE = 8538; AIC + **35904.03** TABULATED

	h_0	h_1	h_2	h_3	h_4
g_0	539.33	620.29	614.60	562.20	589.71
g_0 spatial	531.70	—	—	—	—
g_1	1044.08	1138.48	1213.57	1098.81	1125.73
g_2	457.31	607.84	557.14	503.70	524.96
g_2 spatial	—	—	0.00	0.97	24.62
g_3	618.53	724.85	737.13	665.43	691.26

TABLE V
DATA SOURCE, UNIT SIZE, AND RESOLUTION MATCH (COARSENED)

Source	Trimmed	Unit Area	Processed	Variable
LCDS	1935×5400	$4' \times 4'$		F
GPWv3	3432×8640	$2.5' \times 2.5'$	$20' \times 20'$	N
GTOPO30	15480×43200	$30'' \times 30''$	$(\approx 37 \times 37 \text{ km})$	R

LCDS: Land Cover Data Set based on NOAA data in 1990

GPWv3: Gridded Population of the World Version 3, available at CIESIN
GTOPO30: available at USGS

model is inferior to the spatial model $g_2 + h_2$. This subtraction makes the comparison easier.

AIC values for the independent models as well as for the spatial models are significantly improved by the eLogit transformation. Independent models show different ranking results, but the best three models— $g_2 + h_2$, $g_2 + h_3$, and $g_2 + h_4$ —remain the same. (The possible reasons for the superiority of spatial models are discussed in Section VII.) We, therefore, employed the eLogit analysis in the forested regions of East Asia (Section VI). The best, second best, and third best AICs are colored red, blue, and green, respectively. The value of the spatial step function is written in magenta.

The respective AIC values in Table IV are less than those in Table III. This implies that additive model (3) of the two effects of $g(N)$ and $h(R)$ fits the Hiroshima data after the eLogit transformation. This improvement can be explained by the interaction between the human population and the slope for forest ratio F . It is easily imagined that steep slopes inhibit extensive cultivation and other activities.

V. WORLD DATA SET AND TEST AREAS

The formulas obtained from the Japanese data were then applied to the East Asia data. Table V shows the data sources used to make up F , N , and R . To the best of our knowledge, we believe that the Gridded Population of the World (GPW) [16]–[18] is the only source of spatial human population distributions on a worldwide grid-cell basis. The newest version (GPWv3) was used in this paper.

The source code of the data preparation and the analyses are available through the World Wide Web.¹

A. Resolution Matching on the Same Grid-Cell Location

Data on water surfaces and missing cells were excluded from the cell-aggregation process. The original values were aggregated in a coarsened larger cell of $20' \times 20'$, the resolution

¹<http://www.cis.shimane-u.ac.jp/~tanaka>

TABLE VI
ACTUAL WORLD DATASET USED IN THE ANALYSIS

Forest Ratio ($0 < F \leq 1$)	Population Density	Relief energy (m)
0.320000	97.6875	1061
0.920000	2.2500	1893
0.880000	2.6250	1179
1.000000	3.6875	951
0.708333	2.0000	463
:	:	:

used for calculating the forest areal ratio by the following formula:

$$F(s) = \frac{\sum_{i=1}^{25} I(c_i \in K)}{25}$$

where K denotes the set of class codes (category identifier) of forests, and c_i is the identifier of the i th original cell. F includes open forest, i.e., forest or shrubland, which is both evergreen and deciduous, needleleaf, and broad leaf, $0 < \text{class code} < 130$ as defined by the Land Cover Data Set (LCDS) [19].

There are many data sources on the global land cover such as the International Geosphere Biosphere Programme's Data and Information System Global 1-km LCDS: DISCover [20]. Most of these data sets are based on uniform acreage cells. For the purpose of data aggregation with the GPW, those data must be interpolated to match the GPW cell system based on equal latitude-longitude minute divisions. We, therefore, used the LCDS data set available at the United Nations Environment Programme Global Resource Information Database Tsukuba.² The data set is based on the 1990 National Oceanic and Atmospheric Administration satellite observations and is suitable for cross-sectional analysis with GPWv3.

We used the following formula for N :

$$N(s) = \frac{\sum_{i=1}^{16} n_{\text{org}_i}}{16 - m}$$

where n_{org_i} is the population density of the original unit cell, and m denotes the number of the missing values such as water surfaces [18]. We used the following equation for R :

$$R(s) = \max(r_{\text{org}_i} : i = 1, \dots, 1600) - \min(r_{\text{org}_i} : i = 1, \dots, 1600)$$

where r_{org_i} is the altitude of the original unit cell of Global Topographic data in 30-arcsec units [21].

Table VI shows the resultant data set for the analysis. Each row corresponds to values in the same aggregated cell on the same location.

The relative appropriateness to the actual data of the relations is

$$E[L] = I(s \in A) \{ \beta_0 + g_k(N) + h_l(R) \} \quad (13)$$

where s is a site location, A indicates the forested area, A^c indicates the water surface, desert, and forest limit, and k and l are form identifiers (see Table II) and are to be compared with the test area hereafter. Step functions give the basic criteria

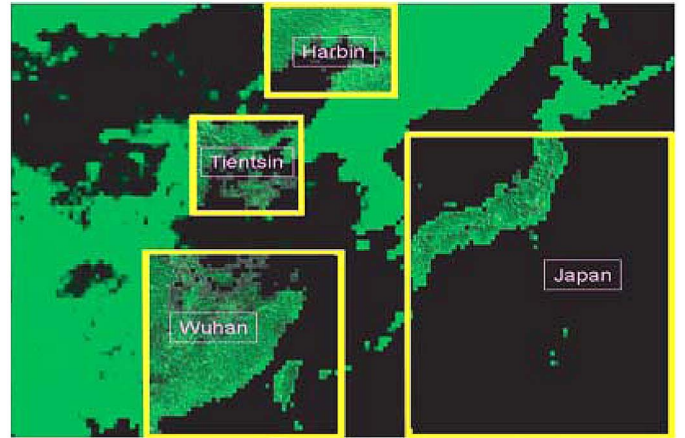


Fig. 9. Test areas in East Asia.

TABLE VII
LOCATIONS AND RESOLUTIONS OF TEST AREAS

Name	Upper	Lower	Left	Right	Resolution
Harbin	N50°	N43°	E120°	E128°	21 × 24
Tientsin	N42°	N35°	E113°	E123°	21 × 30
Wuhan	N33°	N20°	E110°	E125°	39 × 45
Japan	N41°	N20°	E130°	E150°	63 × 60

TABLE VIII
AIC EVALUATION OF MODELS $L = \beta_0 + g_k(N) + h_l(R)$; HARBIN
($0 < F \leq 1$, SAMPLE SIZE = 375; AIC + 1420.85 TABULATED)

	h_0	h_1	h_2	h_3	h_4
g_0	199.38	172.47	196.85	208.12	233.74
g_0 spatial	93.46	—	—	—	—
g_1	202.27	188.72	210.50	203.65	250.47
g_2	203.53	190.62	210.32	207.58	209.50
g_2 spatial	—	—	0.00	53.92	61.37
g_3	204.36	190.63	211.34	205.45	207.21

of appropriateness for comparing candidates to obtain tractable functional forms.

B. Test Area Selection

Fig. 9 depicts the test areas listed in Table VII. We selected four different regions in East Asia.

VI. MODEL SELECTION IN THE TEST AREAS

Tables VIII–XI list the analysis results in the Asian test areas. Note that the respective AIC values of $g_2(N) + h_2(R)$ with dependent errors are set to zero as comparative control criteria. For the estimation of step functions $g_0(N)$ and $h_0(R)$, we prepared ten intervals with equal sample sizes in the respective intervals for each function.

There was a dramatic improvement in the spatial models. The models indicate apparently better relative appropriateness to the data in all of the areas.

Except for Table XI, the nonlinear spatial models with a limited number of parameters show better relative appropriateness to the data than the step functions. For the human factor, form g_2 best reveals the likely quantitative features of forest–human interrelations among the others; a less clear trend can be observed for slope factor R .

²<http://www-cger.nies.go.jp/grid-j/gridtxt/gflcds.html>

TABLE IX

AIC EVALUATION OF MODELS $L = \beta_0 + g_k(N) + h_l(R)$; TIENTSIN
($0 < F \leq 1$, SAMPLE SIZE = 391; AIC + 1210.63 TABULATED)

	h_0	h_1	h_2	h_3	h_4
g_0	188.18	305.21	192.57	249.98	305.21
g_0 spatial	107.63	—	—	—	—
g_1	186.45	212.23	205.93	197.92	243.72
g_2	171.61	218.70	196.20	203.11	213.02
g_2 spatial	—	—	0.00	15.72	-0.62
g_3	212.75	212.75	206.65	222.78	222.68

TABLE X

AIC EVALUATION OF MODELS $L = \beta_0 + g_k(N) + h_l(R)$; WUHAN
($0 < F \leq 1$, SAMPLE SIZE = 949; AIC + 3412.99 TABULATED)

	h_0	h_1	h_2	h_3	h_4
g_0	750.26	826.80	735.27	899.51	812.36
g_0 spatial	283.29	—	—	—	—
g_1	738.80	761.80	736.68	734.39	862.99
g_2	735.73	800.38	736.53	834.45	1013.37
g_2 spatial	—	—	0.00	8.86	57.00
g_3	771.07	874.06	754.67	837.23	885.67

TABLE XI

AIC EVALUATION OF MODELS $L = \beta_0 + g_k(N) + h_l(R)$; JAPAN
($0 < F \leq 1$, SAMPLE SIZE = 354; AIC + 1586.15 TABULATED)

	h_0	h_1	h_2	h_3	h_4
g_0	70.53	45.99	41.90	120.16	42.21
g_0 spatial	-38.55	—	—	—	—
g_1	43.29	37.03	30.46	28.88	28.40
g_2	35.80	51.80	24.87	20.83	72.71
g_2 spatial	—	—	0.00	1.13	50.58
g_3	56.90	29.91	20.81	62.93	84.16

TABLE XII

ESTIMATED PARAMETERS BY TEST AREA: $g_2(N) + h_2(R)$ SPATIAL

Param.	Harbin	Tientsin	Wuhan	Japan
β_0	0.0562	-0.1297	0.3297	0.7163
β_1	0.3742	0.3556	0.6819	27.07
β_2	11.42	53.44	6.738	12.41
β_3	3.408	9.175	1.574	1.004
δ	0.2987	0.7092	0.1808	0.1541
θ	65.71	646.8	59.01	199.0
ϕ	0.2509	0.2491	0.2480	0.1874
σ^2	0.6845	0.4993	0.4165	0.07191
$\sigma^2(\phi)$	0.0954	0.1611	0.1040	0.06177

VII. DISCUSSION

It is reported that adjacency to developed land and proximity to transportation networks and major human settlements are important factors that determine regional patterns of land development [22]. As the fragmentation and the dispersion of forests should be taken into account, it is quite reasonable that spatial models dramatically improve the relative appropriateness of the model to the data.

Table XII reveals the difference between Japan and China. The last two rows in the China data show that $\hat{\sigma}^2$ are greatly improved by $\hat{\sigma}^2(\hat{\phi})$. This implies the apparent superiority of the dependent error models. In Japan, however, the fitted model with independent errors is already fine, and, hence, the spatial model improves the independent model only a little.

Furthermore, from the values of δ and θ , we can see that Tientsin seems different than other areas. Relatively flat areas

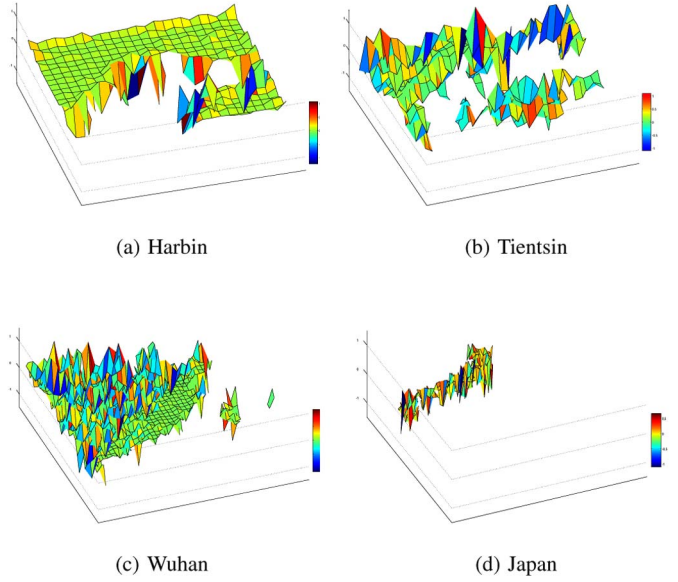


Fig. 10. Conditional error displays [model: $L = \beta_0 + g_2(N) + h_2(R)$]. (a) Harbin. (b) Tientsin. (c) Wuhan. (d) Japan

are almost completely deforested; forests appear resistant on the upward gradient, whereas forests rapidly disappear before an areal population increase. It could be imagined that forests should barely remain in the surrounding steep hillsides, the large flat areas be entirely cultivated, and the densely populated areas be urban cities in the forelands.

Our test area of Tientsin encompassed the Hebei (Hopeh) Province, and the general literature³ supports this observation: The North China Plain gently slopes from west to east. It is bounded by the Yen Mountains on the north, the T'ai-hang Mountains to the west, and the Gulf of Chihli to the east. The Great Wall zigzags along the crests of the Yen Mountains. Between the Yen Mountains are large basin plains, which are cultivated and well inhabited. Beyond these mountains, the Mongolian Plateau stretches from the north part of the Hebei Province. The rim of the plateau has an average elevation of 3900–4900 ft and is rugged and inhospitable to human settlement.

These observations must be bolstered in the future with more detailed geographical information and field research.

Fig. 10 shows spatial conditional error displays. The figures are depicted according to residuals calculated by $F_{xy} - \hat{F}_{xy}$, where $\hat{F}_{xy} = 1.5 - 2/[1 + \exp\{\hat{L}_{xy}\}]$ is a value predicted by the spatial eLogit model (11): $\hat{L}_{xy} = \hat{\mu}_{xy} + \phi(e_{x+1,y} + e_{x-1,y} + e_{x,y+1} + e_{x,y-1})$. Here, $\hat{\mu}_{uv} = \beta_0 + \hat{g}_k(N_{uv}) + \hat{h}_l(R_{uv})$, $e_{uv} = L_{uv} - \hat{\mu}_{uv}$, and (u, v) denotes the site location.

A. Implication of the Models

We believe that the parameters could be plain environmental indicators if we compare them by area. Namely, if the coefficients are estimated by region with the suffix d and year-by-year (t), then $\beta = \beta_d(t)$.

- Cross-sectional comparative comprehension can be visualized at $t = t_c$ with a scatter plot, $\beta_d(t_c)$, with $d = 1, 2, \dots, D$, where D is the total number of surveyed districts.

³<http://www.britannica.com>

- Time-series trends can be observed for an area $d = k$ by overplotting $\beta_k(t_1), \beta_k(t_2), \dots$ with tracing arrows.

If an improvement in the chronological values of β_k in an area is observed, then the environmental policy for that area can be deemed successful.

Agenda 21 includes specific activities such as collecting, compiling, and regularly updating and distributing information on land classification and land use, including data on forest cover, areas suitable for reforestation, endangered species, ecological values, traditional/indigenous land-use values, biomass, and productivity, correlating demographic, socioeconomic, and forest resources information at the microlevel and the macrolevel, and periodic analyses of forest programs [23].

This paper suggests that the typical socioeconomic factors affecting deforestation can be measured and compared by area with the obtained relation.

Test areas must be more precisely defined in terms of their location and size, presumably a disk-shaped area centered on a city area. For large-scale analysis, it would be useful to employ typical climate and apparent economic classifications, such as “developed region in a temperate zone” or “developing region in a tropical zone.”

More functional forms should be explored, in particular, a sigmoid-shaped function such as $\log(N + 1)$ and R to the power of γ , namely, $(\log(N + 1))^\gamma$ and R^γ . Explanatory variables such as income and fire density [24] might well be incorporated to improve the models. However, data availability of the former socioeconomic variable is limited even on the basis of municipal body worldwide, fluctuated by currency rate, and needed to be spatially interpolated to match the grid-cell shape.

Model (13) contains model errors only on the right-hand side of the equation. The GPW population values should contain much larger measurement errors than the forest areal ratios. However, measurement errors also exist on the left side of the equation in F . From this standpoint, mixed models (see, e.g., [25]) are considered to be beneficial for obtaining stable estimates and, thus, should be explored further. Relief energy (R) should also be treated more carefully as a moving average.

This paper shows that human population (N) and slope factor (R) for logit-type transform (L) of forest acreage ratio (F) have the potential to elucidate aspects of deforestation in East Asia and possibly other areas.

APPENDIX I

AIC OF SPATIALLY DEPENDENT MODELS

The parameter estimation and AIC will be derived under the complete data over a rectangular region.

It is known that conditional distributions (11) of L_{xy} in respective sites $s = (x, y)$ uniquely specify the joint distribution of the forest coverage vector \mathbf{L} (see [26, Ch. 6]). The

joint distribution is given by a multivariate normal distribution, i.e.,

$$\mathbf{L} \sim \mathbf{N}_n (\boldsymbol{\mu}, \sigma^2(\mathbf{I}_n - \phi H)^{-1}), \quad n = rc$$

with mean vector $\boldsymbol{\mu} = \boldsymbol{\mu}(\boldsymbol{\beta})$ and variance–covariance matrix $\sigma^2(\mathbf{I}_n - \phi H)^{-1}$, where H is the adjacency matrix. The log-likelihood function, for example, $\ell(\boldsymbol{\beta}, \sigma^2, \phi)$, is, therefore, given by

$$\ell(\boldsymbol{\beta}, \sigma^2, \phi) = -\frac{n}{2} \log(2\pi\sigma^2) + \frac{1}{2} \log |\mathbf{I} - \phi H| - \frac{Q(\boldsymbol{\beta}, \phi)}{2\sigma^2} \quad (14)$$

where

$$Q(\boldsymbol{\beta}, \phi) = \{\mathbf{L} - \boldsymbol{\mu}(\boldsymbol{\beta})\}^T (\mathbf{I} - \phi H) \{\mathbf{L} - \boldsymbol{\mu}(\boldsymbol{\beta})\}. \quad (15)$$

The maximum-likelihood estimators (MLEs) can be obtained by the following procedure.

- S1 Fix ϕ in the interval $(0, \lambda)$, where λ denotes the reciprocal of the maximum eigenvalue of matrix H .
 - S2 Find the optimal regression parameter $\boldsymbol{\beta}$ minimizing the quadratic form $Q(\boldsymbol{\beta}, \phi)$ of (15), and put the solution as $\hat{\boldsymbol{\beta}} = \hat{\boldsymbol{\beta}}(\phi)$.
 - S3 Repeat S1 and S2 for various values ϕ (*grid search*), and find the optimal value maximizing the profile likelihood $\ell(\hat{\boldsymbol{\beta}}(\phi), \hat{\sigma}^2(\phi), \phi)$. Put the solution as $\hat{\phi}$.
 - S4 MLEs of $(\phi, \boldsymbol{\beta}, \sigma^2)$ are obtained by $(\hat{\phi}, \hat{\boldsymbol{\beta}}(\hat{\phi}), \hat{\sigma}(\hat{\phi}))$.
- Concerning S2, $\boldsymbol{\beta}$ is estimated by the following equation:

$$\frac{\partial Q(\boldsymbol{\beta}, \phi)}{\partial \boldsymbol{\beta}} = -2 \{\mathbf{L} - \boldsymbol{\mu}(\boldsymbol{\beta})\}^T (\mathbf{I} - \phi H) \frac{\partial \boldsymbol{\mu}(\boldsymbol{\beta})}{\partial \boldsymbol{\beta}} = 0. \quad (16)$$

For the case of $\mu_{xy}(\boldsymbol{\beta}) = \beta_0 + g_2(N_{xy}) + h_3(R_{xy})$ in Table II, the derivative $\partial \boldsymbol{\mu}(\boldsymbol{\beta}) / \partial \boldsymbol{\beta}$ becomes the matrix shown at the bottom of the page.

The solution of (16) is generally derived by an iterative procedure. If the regression function is given by the step function $\mu_{xy}(\boldsymbol{\beta}) = \beta_0 + g_0(N_{xy}) + h_0(R_{xy})$, with $\boldsymbol{\beta} = (\beta_0, \omega_2, \dots, \omega_{16}, \psi_2, \dots, \psi_9)^T$, all entries of the matrix $\partial \boldsymbol{\mu}(\boldsymbol{\beta}) / \partial \boldsymbol{\beta}$ are 0 or 1. In this case, the equation reduces to a linear equation, and the exact solution is found noniteratively.

Finally, AIC (12) is obtained by the use of the estimated parameters. Note that the first four terms of AIC (12) are obtained by the ordinary AIC for transformed ratio \mathbf{L} , and the last two terms are due to the derivatives of the variable transformation from F_{xy} to L_{xy} .

APPENDIX II NONRECTANGULAR REGION CASE

The adjacent matrix H^* with 15 observed data in Fig. 8 is shown at the top of the next page. This adjacent matrix is expressed by $H^* = P^T H P$, where H is the adjacent matrix

$$\begin{pmatrix} 1 & \frac{\partial g_2(N_{1,1})}{\partial \beta_1} & \dots & \frac{\partial g_2(N_{1,1})}{\partial \beta_3} & \frac{\partial h_3(R_{1,1})}{\partial \gamma_1} & \dots & \frac{\partial h_3(R_{1,1})}{\partial \gamma_3} \\ \vdots & \vdots & & \vdots & \vdots & & \vdots \\ 1 & \frac{\partial g_2(N_{r,c})}{\partial \beta_1} & \dots & \frac{\partial g_2(N_{r,c})}{\partial \beta_3} & \frac{\partial h_3(R_{r,c})}{\partial \gamma_1} & \dots & \frac{\partial h_3(R_{r,c})}{\partial \gamma_3} \end{pmatrix} : n \times 7$$

$$H^* = \left(\begin{array}{ccccccccc} 0 & 1 & 0 & 0 & 0 \\ 1 & 0 & 1 & 1 & 0 \\ 0 & 1 & 0 & 0 & 1 \\ 0 & 1 & 0 & 0 & 1 & 0 & 1 & 0 \\ 0 & 0 & 1 & 1 & 0 & 0 & 0 & 0 \\ 0 & 0 & 0 & 1 & 0 & 0 & 0 & 0 & 0 \\ 1 & 0 & 1 & 0 & 0 & 1 & 0 & 0 & 0 \\ 0 & 0 & 0 & 0 & 0 & 0 & 0 & 1 & 1 \\ 0 & 1 & 0 & 0 & 0 & 0 & 1 & 0 & 0 \\ 0 & 0 & 1 & 0 & 0 & 1 & 0 & 0 & 0 \\ 0 & 0 & 0 & 1 & 0 & 0 & 0 & 0 & 1 \\ 1 & 0 & 0 & 1 & 0 & 0 & 1 & 0 & 0 \\ 0 & 1 & 0 & 0 & 1 & 0 & 0 & 0 & 1 \\ 0 & 0 & 1 & 0 & 0 & 0 & 1 & 0 & 0 \\ 0 & 0 & 0 & 1 & 0 & 0 & 0 & 0 & 1 \end{array} \right) : 15 \times 15$$

$$P = \begin{pmatrix} 1 & 0 & 0 \\ 0 & 1 & 0 \\ 0 & 0 & 1 \\ 0 & 0 & 0 \\ & 0 & 0 \\ & 1 & 0 \\ & 0 & 1 \\ & 0 & 0 \\ & 1 & 0 & 0 \\ & 0 & 1 & 0 \\ & 0 & 0 & 0 \\ & 0 & 0 & 1 \\ & 0 & 0 & 0 \\ & 1 & 0 & 0 \\ & 0 & 1 & 0 \\ & 0 & 0 & 0 \\ & 0 & 0 & 1 \\ & 0 & 0 & 0 \\ & 1 & 0 & 0 \\ & 0 & 1 & 0 \\ & 0 & 0 & 1 \\ & 0 & 0 & 0 \\ & 1 & 0 & 0 \\ & 0 & 1 & 0 \\ & 0 & 0 & 1 \end{pmatrix} : 20 \times 15$$

of the complete data defined by (9), and P is a matrix shown at the top of the page. Matrix P plays a role in selecting the pixels from the complete data. Thus, the adjacency matrix with missing data can be obtained with fewer memory requirements because the matrix of the rectangular data is easily found by taking the Kronecker product.

The joint distribution of the eLogit-transformed ratio vector \mathbf{L} is similarly derived, and AIC is obtained by

$$\begin{aligned} \text{AIC} = & n \log(2\pi e) + n \log \hat{\sigma}^2 - \log |\mathbf{I}_n - \hat{\phi} H^*| + 2p \\ & - 2n \log 2 + 2 \sum_{x,y}^* \log \{(F_{xy} + 0.5)(1.5 - F_{xy})\} \end{aligned}$$

where the sum $\sum_{x,y}^*$ extends over n observed pixels.

ACKNOWLEDGMENT

The authors would like to thank Prof. C. Hall of the State University of New York, Prof. R. Tateishi of Chiba University, and Prof. R. Shibasaki and Prof. M. Nakayama of the University

of Tokyo for their knowledge about the literature and the data used in this paper; Y. Ikeda, a former student of Shimane University, for his elaboration on formulating the worldwide data set; J. Fan, a masters degree student of Shimane University, for his guidance on pronouncing Chinese place names in English; and the editors and reviewers who gave valuable comments and suggestions.

REFERENCES

- [1] X. Jin, J. Li, C. C. Schmidt, T. J. Schmit, and J. Li, "Retrieval of total column ozone from imagers onboard geostationary satellites," *IEEE Trans. Geosci. Remote Sens.*, vol. 46, no. 2, pp. 479–488, Feb. 2008.
 - [2] J. R. Wang, L. A. Chang, B. Monosmith, and Z. Zhaonan, "Water vapor profiling from CoSSIR radiometric measurements," *IEEE Trans. Geosci. Remote Sens.*, vol. 46, no. 1, pp. 137–145, Jan. 2008.
 - [3] C. Ruf and A. Wamock, "GEOSAT follow-on water vapor radiometer: Performance with a shared active/passive antenna," *IEEE Trans. Geosci. Remote Sens.*, vol. 45, no. 4, pp. 970–977, Apr. 2007.
 - [4] S. Cros, A. Chanzy, M. Weiss, T. Pellarin, J.-C. Calvet, and J. P. Wigneron, "Synergy of SMOS microwave radiometer and optical sensors to retrieve soil moisture at global scale," *IEEE Trans. Geosci. Remote Sens.*, vol. 46, no. 4, pp. 835–845, Mar. 2008.

- [5] E. Lambin, "Modelling and monitoring land-cover change processes in tropical regions," *Prog. Phys. Geogr.*, vol. 21, no. 3, pp. 375–393, 1997.
- [6] N. Myers, "The world's forests and human populations: The environmental interconnections," *Popul. Dev. Rev.*, vol. 16, pp. 1–15, 1990. (supplement).
- [7] P. Cottle, "Insuring Southeast Asian commercial forests: Fire risk analysis and the potential for use of data in risk pricing and reduction of forest fire risk," *Mitig. Adapt. Strategies Glob. Chang.*, vol. 12, no. 1, pp. 181–201, Jan. 2007.
- [8] S. Tanaka and R. Nishii, "Incorporation of human dimension into the analysis of remotely-sensed images: A spatial model of deforestation," in *Proc. IGARSS*, 1999, pp. 922–924.
- [9] S. Tanaka and R. Nishii, "Verification of deforestation in East Asia by spatial logit models due to population and relief energy," in *Proc. 12th SPIE Eur. Int. Symp. Remote Sens.*, 2005, vol. 5976, pp. 597 60W-1–597 60W-10.
- [10] S. Tanaka and R. Nishii, "Extended spatial logit models of deforestation due to population and relief energy in East Asia," in *Proc. SPIE Remote Sens.*, 2006, vol. 6359, pp. 63 590G-1–63 590G-8.
- [11] S. Tanaka and R. Nishii, "Deforestation due to population and relief energy through spatially-correlated logit models," in *Proc. IGARSS*, 2007, pp. 2310–2313.
- [12] S. Tanaka and R. Nishii, "Non-linear regression models to identify functional forms of deforestation," in *Proc. IGARSS*, 2008, pp. IV49–IV52.
- [13] S. Tanaka, "A quantitative aspect on man–land interrelations: Case study of deforestation in Japan," *Ecol. Eng.*, vol. 4, pp. 163–172, 1995.
- [14] R. Nishii, "Asymptotic properties of criteria for selection of variables in multiple regression," *Ann. Stat.*, vol. 12, no. 2, pp. 758–765, 1984.
- [15] H. Akaike, "Information theory and an extension of the maximum likelihood principle," in *Proc. 2nd Int. Symp. Inf. Theory*, 1973, pp. 267–281.
- [16] W. Tobler, U. Deichmann, J. Gottsegen, and K. Maloy, "World population in a grid of spherical quadrilaterals," *Int. J. Popul. Geogr.*, vol. 3, no. 3, pp. 203–225, Sep. 1997.
- [17] U. Diechmann, D. L. Balk, and G. Yetman, "Transforming population data for interdisciplinary usages: From census to grid," in *Proc. CIESIN*, 2001, pp. 1–19.
- [18] D. L. Balk, U. Deichmann, G. Yetman, F. Pozzi, S. I. Hay, and A. Nelson, "Determining global population distribution: Methods, applications and data," *Adv. Parasitol.*, vol. 62, pp. 119–156, 2006.
- [19] "AARS global 4-minute land cover data set," *CEReS*, 1997, Chiba Univ.
- [20] A. S. Belward, J. E. Estes, and K. Kline, "The IGBP-DIS global 1-km land-cover data set DISCover: A project overview," *Photogramm. Eng. Remote Sens.*, vol. 65, no. 9, pp. 1013–1020, 1999.
- [21] *Digital Elevation Models: Data Users Guide 5*, U.S. Geological Survey, Nat. Mapping Program, Reston, VA, 1993.
- [22] C. A. S. Hall, H. Tian, Y. Qi, G. Pontius, and J. Cornell, "Modeling spatial and temporal patterns of tropical land use change," *J. Biogeogr.*, vol. 22, pp. 753–757, 1995.
- [23] United Nations, *Agenda 21 Forest Principles (Draft Rio Declaration)*, 1992, New York: United Nations Publ.
- [24] D. K. Davies, S. Ilavajhala, M. M. Wong, and C. O. Justice, "Fire information for resource management system: Archiving and distributing MODIS active fire data," *IEEE Trans. Geosci. Remote Sens.*, vol. 47, no. 1, pp. 72–79, Jan. 2009.
- [25] W. Fuller, *Measurement Error Models*. New York: Wiley, 1987.
- [26] N. Cressie, *Statistics for Spatial Data*. New York: Wiley, 1991.



Shojiro Tanaka (M'89) received the Ph.D. degree from Hiroshima University, Hiroshima, Japan, in 1992.

He is currently a Professor with the Faculty of Science and Engineering, Shimane University, Matsue, Japan. His research interests include modeling of environments, remote sensing, and spatiotemporal extension of data models in database management systems.



Ryuei Nishii (M'96) received the Ph.D. degree from Hiroshima University, Hiroshima, Japan, in 1981.

He is currently a Professor with the Faculty of Mathematics, Kyushu University, Fukuoka, Japan. His research interests include statistics, particularly the classification of geostatistical data based on statistical or machine learning approaches.